$CsBi_4Te_6$: A High-Performance Thermoelectric Material for Low-Temperature Applications

Duck-Young Chung,[1] Tim Hogan,[2] Paul Brazis,[3] Melissa Rocci-Lane,[3] Carl Kannewurf,[3] Marina Bastea,[4] Ctirad Uher,[4] Mercouri G. Kanatzidis[1]*

Thermoelectric (Peltier) heat pumps are capable of refrigerating solid or fluid objects, and unlike conventional vapor compressor systems, they can be miniaturized without loss of efficiency. More efficient thermoelectric materials need to be identified, especially for low-temperature applications in electronics and devices. The material $CsBi_4Te_6$ has been synthesized and its properties have been studied. When doped appropriately, it exhibits a high thermoelectric figure of merit below room temperature (ZT_{max} ~0.8 at 225 kelvin). At cryogenic temperatures, the thermoelectric properties of $CsBi_4Te_6$ appear to match or exceed those of $Bi_{2-x}Sb_xTe_{3-y}Se_y$ alloys.

A broad search is under way to identify new materials with enhanced thermoelectric (TE) properties (*1–3*). Important applications include cooling of electronic circuitry and superconducting devices. Particularly desirable are candidate materials that function well at or below room temperature, with performance characteristics better than those of the well-known $Bi_{2-x}Sb_xTe_{3-y}Se_y$ alloys (*4*). Until recently, most investigations focused on tuning (*5*) the composition of these alloys, doping (*6*) with other heavy metals, and optimizing device design. Several classes of materials are currently under investigation, including skutterudites (*7*), half-Heusler alloys (*8*), clathrates (*9*), and pentatellurides (*10*).

We have explored materials with more complex compositions and structures that would likely have complex electronic structures that could give rise to high TE performance (*11*). Good TE materials require an unusual combination of electrical and thermal properties. The challenge lies in achieving simultaneously high electrical conductivity σ, high TE power S, and low thermal conductivity κ, which define the unitless TE figure of merit $ZT = (S^2\sigma/\kappa)T$ (where T is temperature). All three of these properties are determined by the details of the electronic structure (band gap, band shape, and band degeneracy near the Fermi level) and scattering of charge carriers (electrons or holes) and thus are not independent. The total thermal conductivity κ also has a contribution from the phonon thermal conductivity, κ_l, such that $\kappa = \kappa_e + \kappa_l$, where κ_e is the carrier thermal conductivity.

Recently we reported that $K_2Bi_8S_{13}$ (*12*) and β-$K_2Bi_8Se_{13}$ (*13*) have promising TE properties and particularly low κ values (*14, 15*). The alkali metals play an important role in reducing the total κ. When we moved on to investigate corresponding Te analogs with Cs, we obtained an unexpected result: Instead of $Cs_2Bi_8Te_{13}$, we isolated $CsBi_4Te_6$. From a chemical point of view, this amounts to a reduction of a Bi_2Te_3 unit by a half-equivalent of electrons. The added electrons, however, result in a complete restructuring of the Bi_2Te_3 framework so that the new structure bears no resemblance to the corresponding binary compound. The new compound seems to be an outstanding candidate for low-temperature TE applications. We describe here the synthesis, structure, and TE properties of $CsBi_4Te_6$, which, when doped appropriately, achieves a maximum ZT of ~0.8 at 225 K, making it the best bulk TE material below room temperature.

We first obtained $CsBi_4Te_6$ by reacting Cs_2Te and Bi_2Te_3 at 700°C. Subsequently we devised a synthesis from the direct stoichiometric combination of the elements at 600°C. The material is stable in air and water, and melts without decomposition at 545°C. The crystals grow with long needle-like morphology (Fig. 1A). The direction of rapid growth along the needle axis is also the direction of maximum TE performance.

$CsBi_4Te_6$ has a layered anisotropic structure (*16*). It is composed of anionic $[Bi_4Te_6]$ slabs alternating with layers of Cs^+ ions (Fig. 1B). The addition of one electron per two equivalents of Bi_2Te_3 is not topotactic and does not produce a formal intercalation compound, but causes a complete reorganization of the bismuth telluride framework to produce a new structure type. The added electrons localize on the Bi atoms to form Bi-Bi bonds that are 3.238 ± 0.001 Å long. The presence of these bonds is unusual in bismuth chalcogenide chemistry, and it is not clear whether they play a role in the enhanced TE properties of the material (*17*). The $[Bi_4Te_6]$ layers are strongly anisotropic, as they consist of one-dimensional (1D) $[Bi_4Te_6]$ lath-like ribbons running parallel to the b axis. The width and height of these laths is 23 Å by 12 Å (Fig. 1C). The laths arrange side by side and are connected via the Bi-Bi bonds mentioned above. This structural feature is responsible for the strongly 1D needle-like appearance of the $CsBi_4Te_6$ crystals. The Bi atoms are octahedrally surrounded either by six Te atoms or by five Te atoms and one other Bi atom. The degree of distortion around the Bi atoms is relatively small. The longest and shortest Bi-Te bonds are 3.403 ± 0.001 Å and 2.974 ± 0.001 Å, respectively, with an average distance of 3.18 Å. The Cs^+ ions lie between the $[Bi_4Te_6]$ layers, and their atomic displacement parameters are 1.6 times those of the Bi and Te atoms, which suggests that they undergo considerable "rattling" motion (*18*). Such a dynamic motion in the lattice can be responsible for strong scattering of heat-carrying phonons and leads to low κ values (see below) (*19*). The immediate environment of Cs is a square prismatic arrangement of Te atoms.

As obtained directly from the synthesis (with no deliberate attempt at doping), crystals of $CsBi_4Te_6$ have high room-temperature σ values, ranging from 900 to 2500 S/cm (*20*) (Fig. 2A), and S values from 90 to 120 μV/K (*21*) (Fig. 2B). At lower temperatures, S typically exhibits a maximum of 120 μV/K at ~240 K and then slopes toward zero at 0 K. The κ measurements on a large number of pressed pellets (>97% theoretical density) or oriented ingots (*22*) show values between 1.25 and 1.85 W/m·K, for lightly and heavily doped samples, respectively. These values give rise to relatively high room-temperature ZT values of 0.2 to 0.5; these figures of merit suggest that the material is an excellent candidate for further optimization via chemical manipulation (such as doping, solid solution, and crystal growth). On the basis of the maximum values of S, the band gap of $CsBi_4Te_6$ can be estimated from the formula $E_g \sim 2S_{max} \cdot T_{max}$ (*23*) to be between 0.05 and 0.11 eV.

Because of the promising properties of $CsBi_4Te_6$, we pursued doping studies of this material with various chemical doping agents. We investigated SbI_3, BiI_3, and In_2Te_3 in amounts varying from 0.02 to 4 mole percent. These dopants were chosen for the purpose of placing halide atoms in the Te

[1]Department of Chemistry, Michigan State University and Center for Fundamental Materials Research, East Lansing, MI 48824, USA. [2]Electrical and Computer Engineering & Materials Science and Mechanics, Michigan State University, East Lansing, MI 48824, USA. [3]Department of Electrical Engineering and Computer Science, Northwestern University, Evanston, IL 60208, USA. [4]Department of Physics, University of Michigan, Ann Arbor, MI 48109, USA.

*To whom correspondence should be addressed.

sites (to produce *n*-type doping) and In atoms in the Bi sites (to produce *p*-type doping). Doping with these agents does occur, but we currently do not know what sites in the crystal structure are being occupied. Surprisingly, doping with SbI_3 and BiI_3 produces *p*-doped rather than *n*-doped samples. This observation is not consistent with iodine atoms occupying Te sites but instead suggests Sb and Bi atoms on Te sites. The Sb and Bi atoms, having only five electrons, introduce holes in the Te-based valence band. However, In_2Te_3 can produce *n*-type samples (see below). Depending on the type and degree of doping, room-temperature *S* values between +175 μV/K and −100 μV/K were observed. $CsBi_4Te_6$ is amenable to considerable doping manipulation, much like Bi_2Te_3, and thus higher ZT values may be obtainable.

The σ and *S* data were used to calculate the power factors, $S^2\sigma$, for each dopant versus temperature and doping concentration. The best results in this study were obtained with SbI_3. The evolution of power factor as a function of SbI_3 addition is shown in Fig. 3A. From these data, the optimal concentration seems to lie at 0.05% SbI_3. This sample achieved a maximum power factor of ~51.5 μW/cm·K^2 at 184 K. The temperature dependences of σ and *S* of the best sample are shown in Fig. 3B. The *S* maximum was found at ~250 K. The total κ of the doped samples of the material, ~1.48 W/m·K (Fig. 3C) (*24*), is considerably smaller than that of Bi_2Te_3 (at ~1.85 W/m·K) and more comparable to that of the optimized $Bi_{2-x}Sb_xTe_{3-y}Se_y$ alloy (at 1.56 W/m·K) (*25*). The approximate electronic contribution to κ was estimated using the Wiedemann-Franz law (*26*) for metals as $\kappa_e \sim 0.7$ W/m·K. This result suggests that the measured total κ of this material is almost equally composed of the lattice and electronic contributions. Perpendicular to the growth axis (*b* axis), κ was sharply lower (~0.6 W/m·K), which reflects the highly anisotropic nature of $CsBi_4Te_6$.

The ZT for this sample (0.05% SbI_3-doped $CsBi_4Te_6$) and that of the optimized commercial $Bi_{2-x}Sb_xTe_3$ are compared as a function of temperature in Fig. 3D. Along the growth axis, the computed ZT values for $CsBi_4Te_6$ reach a maximum of 0.82 at 225 K and 0.65 at room temperature. In contrast, optimized $Bi_{2-x}Sb_xTe_3$ *p*-type alloy has a peak of ZT ~ 0.95 at room temperature, whereas at 225 K, its ZT drops to 0.58. Both ZT curves are similar in shape, but that of $CsBi_4Te_6$ is shifted (by ~70 K) to lower temperatures. Because the $CsBi_4Te_6$ samples reach optimum performance at a much lower temperature than does $Bi_{2-x}Sb_xTe_3$, we expect that this new material could be exploited for low-temperature applications, particularly in the temperature range where $Bi_{2-x}Sb_xTe_3$ alloy is ineffective. Recent optimization work on *p*-type $Bi_{2-x}Sb_xTe_{3-y}Se_y$ alloys claimed low-temperature (~210 K) ZT_{max} values of 0.64 (*27*).

Preliminary Hall-effect measurements for SbI_3-doped $CsBi_4Te_6$ samples show that carrier concentrations are on the order of 3×10^{18} to 10^{19} cm^{-3} for samples doped at 0.1% and 0.2% SbI_3 (Fig. 4). Hole mobilities calculated from the electrical conductivity and Hall data show exponentially decreasing mobility as the temperature increases. The hole mobilities

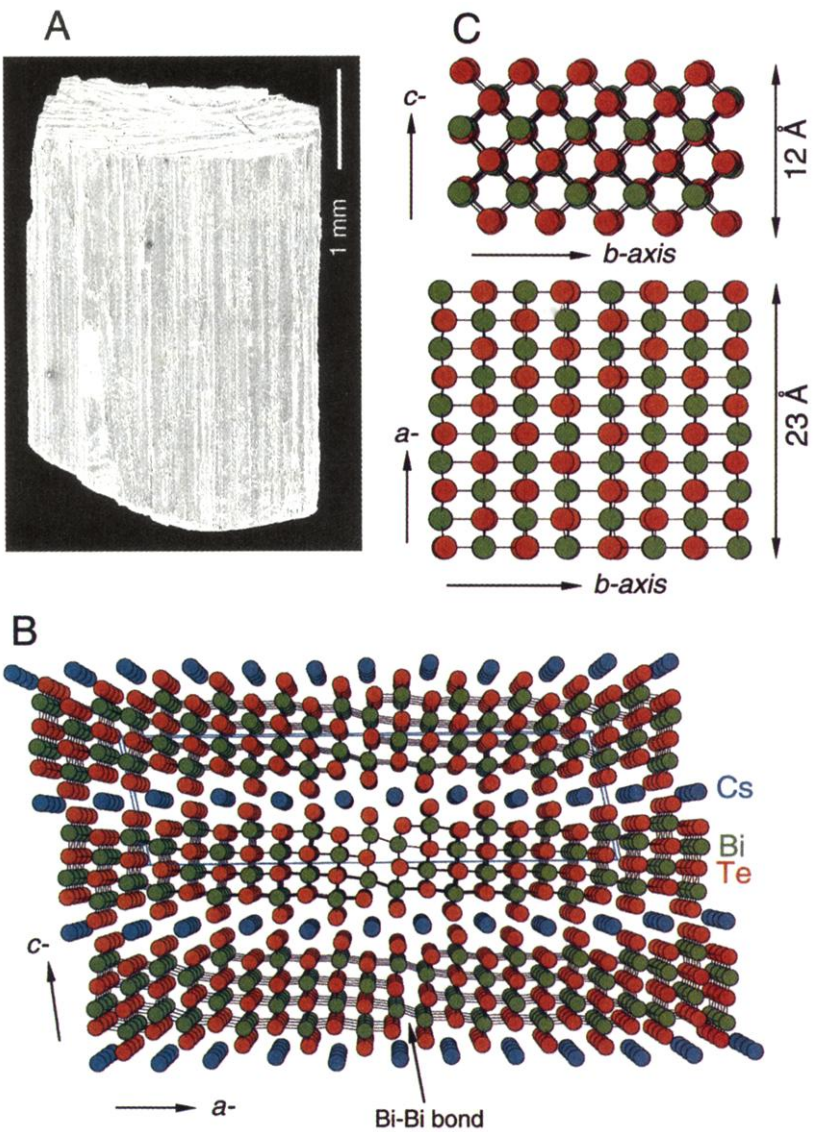

Fig. 1. (**A**) Typical oriented ingot of $CsBi_4Te_6$. The growth axis is along the *b* axis. (**B**) The structure of $CsBi_4Te_6$ looking down the *b* axis. The Bi-Bi bond is indicated by the arrow. (**C**) Individual $[Bi_4Te_6]$ lath (or ribbon) viewed in two different orientations. The laths are joined side by side via Bi-Bi bonds at 3.238 ± 0.001 Å.

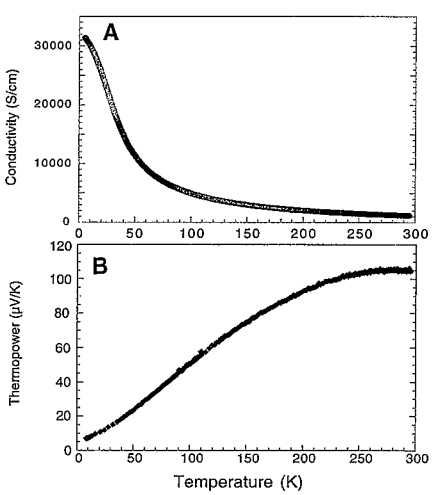

Fig. 2. (**A**) Typical electrical conductivity data of single-crystal $CsBi_4Te_6$ (undoped, as prepared) as a function of temperature. The measurement is along the needle direction. The electrical conductivity was measured using a computer-controlled, four-probe technique. (**B**) Typical thermopower of single-crystal $CsBi_4Te_6$ along the needle axis direction (*b* axis).

in doped $CsBi_4Te_6$ samples range between 700 and 1000 $cm^2/V{\cdot}s$ at room temperature. These are substantially greater than those typically found in the optimized *p*-type bismuth telluride alloy (~380 $cm^2/V{\cdot}s$) (*28*). At low temperatures, the mobilities soar to >5000 $cm^2/V{\cdot}s$. The very high hole mobilities could be due to the 1D character of $CsBi_4Te_6$ and the lack of atomic disorder in its crystal lattice. The carrier concentration shows a weak dependence on temperature, with values decreasing as the temperature is lowered. The carrier concentration tends to diminish as the doping increases away from 0.05% SbI_3, the material with the highest power factor. For these samples, the carrier concentration data could be correlated with the power factor data; the results showed that the power factor decreased as the carrier concentration moved away from 10^{19} cm^{-3} (Fig. 3A).

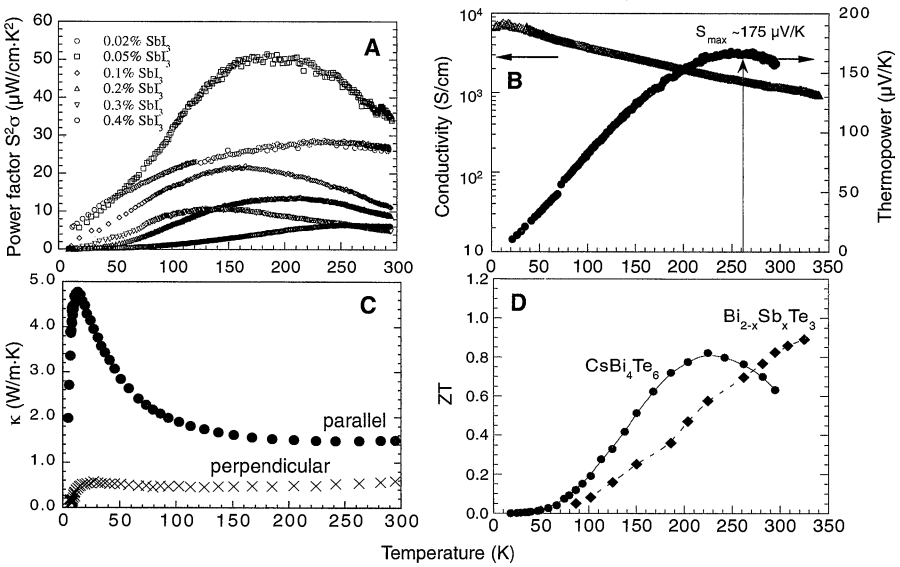

Fig. 3. (**A**) Power factors ($S^2\sigma$) as a function of SbI_3 doping. (**B**) Electrical conductivity and thermopower data of a single crystal of 0.05% SbI_3-doped $CsBi_4Te_6$. (**C**) Total thermal conductivity of an oriented ingot of doped $CsBi_4Te_6$. Data for heat flow parallel and perpendicular to the growth axis (*b* axis) are shown. (**D**) Comparison of ZT versus temperature for 0.05 mol% SbI_3-doped single-crystal $CsBi_4Te_6$ and optimally doped $Bi_{2-x}Sb_xTe_3$ *p*-type alloy (commercial sample obtained from Marlow Industries). The peak maximum for $CsBi_4Te_6$ occurs at ~225 K. ZTs were computed using the thermal conductivity obtained along the growth axis.

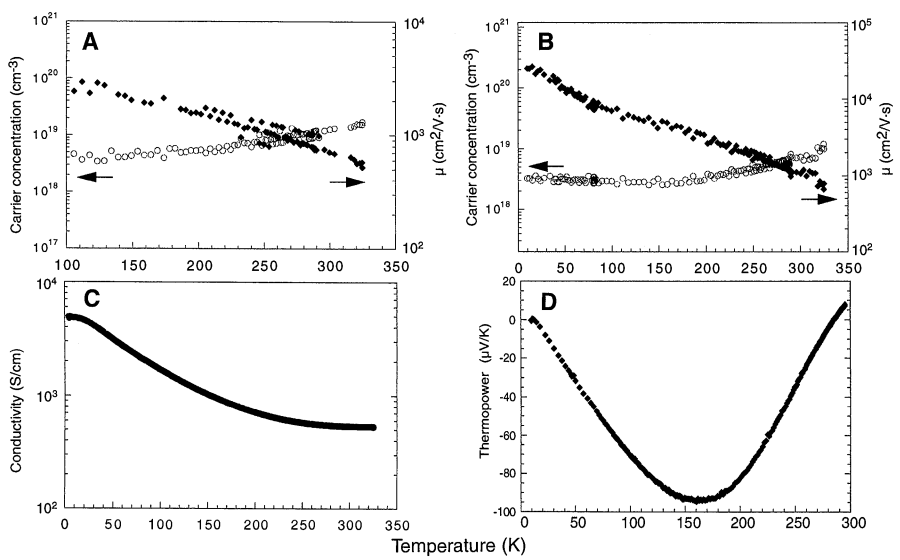

Fig. 4. (**A**) Carrier concentration and hole mobility (μ) as a function of temperature for 0.1 mol% SbI_3-doped $CsBi_4Te_6$ crystals. (**B**) Carrier concentration and hole mobility (μ) as a function of temperature for 0.2 mol% SbI_3-doped $CsBi_4Te_6$. Mobility and carrier concentration data were obtained using dc Hall-effect measurements. Applied current and magnetic field strength were typically 10 mA and 7 kG, respectively. Electrical conductivity and Hall-effect data were taken simultaneously, with mobility values calculated from these data. (**C**) Corresponding electrical conductivity data for In_2Te_3-doped $CsBi_4Te_6$. (**D**) Thermopower data from a single crystal of In_2Te_3-doped $CsBi_4Te_6$.

A complete TE cooling device needs both a *p*-type and an *n*-type version of a material to operate. Thus, an important issue to be addressed in future studies with $CsBi_4Te_6$ is whether *n*-type doping is possible. We have been able to show that In_2Te_3 doping leads to *n*-type charge transport. Not only is *n*-type behavior achievable, but the maximum TE power of −100 μV/K occurs at ~160 K (Fig. 4, C and D), a temperature with important implications for the development of even lower temperature TEs. Although optimum levels have not yet been reached, we believe additional improvements in TE performance in this material are possible with further exploration of doping agents and the investigation of solid solutions such as $CsBi_{4-x}Sb_xTe_6$, $CsBi_4Te_{6-x}Se_x$, and $Cs_{1-x}Rb_xBi_4Te_6$. The latter could result in substantially lower thermal conductivities (as much as 30 to 50% lower), giving projected values of ZT > 1.5. Band structure calculations for $CsBi_4Te_6$ should provide further insight into the electronic properties of this material (*29*).

References and Notes

1. Special issue on Thermoelectric Materials—New Directions and Approaches, T. M. Tritt, M. G. Kanatzidis, H. B. Lyon, G. D. Mahan, Eds., *Mater. Res. Soc. Symp. Proc.* **478** (March 1997).
2. D.-Y. Chung *et al.*, *Mater. Res. Soc. Symp. Proc.* **478**, 333 (1997).
3. F. J. DiSalvo, *Science* **285**, 703 (1999); T. M. Tritt, *Science* **283**, 804 (1999).
4. M. Stordeur, *Phys. Status Solidi* **161**, 831 (1990); H.-H. Jeon, H.-P. Ha, D.-B. Hyun, J.-D. Shim, *J. Phys. Chem. Solids* **4**, 579 (1991); L. R. Testardi, J. N. Bierly Jr., F. J. Donahoe, *J. Phys. Chem. Solids* **23**, 1209 (1962).
5. W. M. Yim and E. V. Fitzke, *J. Electrochem. Soc.* **115**, 556 (1968); ———, F. D. Rosi, *J. Mater. Sci.* **1**, 52 (1966); K. Borkowski and J. Przyluski, *Mater. Res. Bull.* **22**, 381 (1987).
6. S. N. Chizhevskaya and L. E. Shelimova, *Inorg. Mater.* **31**, 1083 (1995); J. Horák, K. Cermák, L. Koudelka, *J. Phys. Chem. Solids* **47**, 805 (1986); P. Lostak, J. Horák, L. Koudelka, *Phys. Status Solidi* **76**, k71 (1983); S. M. Zalar, *Adv. Energy Conv.* **2**, 105 (1962).
7. B. C. Sales, D. Mandrus, R. K. Williams, *Science* **272**, 1325 (1996); B. X. Chen *et al.*, *Phys. Rev. B* **55**, 1476 (1997).
8. C. Uher *et al.*, *Phys. Rev. B* **59**, 8615 (1999); H. Hohl *et al.*, *J. Phys. Cond. Matter* **11**, 1697 (1999); W. Kafer *et al.*, *Inst. Phys. Conf. Ser.* **152**, 185 (1998).
9. G. Nolas, J. L. Cohn, G. Slack, S. B. Schujman, *Appl. Phys. Lett.* **73**, 178 (1998).
10. R. T. Littleton *et al.*, *Appl. Phys. Lett.* **72**, 2056 (1998).
11. Complex electronic structures have a higher probability of producing high thermopower. According to the Mott formula, the thermopower *S* is given by

$$S = \frac{\pi^2}{3} \cdot \frac{k^2 T}{e} \cdot \left. \frac{d[\ln \sigma(E)]}{dE} \right|_{E = E_f}$$

where $\sigma(E)$ is the electrical conductivity determined as a function of band filling, and the electronic conductivity $\sigma = \sigma(E)|_{E=E_f}$ (where E_f is the Fermi energy). If the carrier scattering is independent of energy, then $\sigma(E)$ is just proportional to the density of states at *E*. In the general case, *S* is a measure of the difference in $\sigma(E)$ above and below the Fermi surface—specifically, through the logarithmic derivative $\sigma(E)$ with respect to *E*. Therefore, a material

with an electronic structure complex enough to maximize $d[\ln \sigma(E)]/dE$ will be a good candidate for consideration.
12. M. G. Kanatzidis *et al.*, *Chem. Mater.* **8**, 1465 (1996); B. Chen, C. Uher, L. Iordanidis, M. G. Kanatzidis, *Chem. Mater.* **9**, 1655 (1997).
13. D.-Y. Chung *et al.*, *Chem. Mater.* **9**, 3060 (1997).
14. D.-Y. Chung *et al.*, *Proceedings of the 16th International Conference on Thermoelectrics* (Dresden, Germany, 1997), p. 459.
15. J. L. Schindler *et al.*, *Mater. Res. Soc. Symp. Proc.* **478**, 327 (1997).
16. Single-crystal x-ray diffraction data for $CsBi_4Te_6$ were collected at 293 K on a Siemens SMART Platform charge-coupled device diffractometer. Data are as follows: monoclinic $C2/m$ (no. 12); a = 51.9205 ± 0.0008 Å, b = 4.4025 ± 0.0001 Å, c = 14.5118 ± 0.0003 Å, β = 101.480 ± 0.001°, Z = 8, V = 3250.75 ± 0.11 Å^3, d_{calc} = 7.09 g/cm^3; μ = 55.90 mm^{-1}, 1.43° < θ (Mo K_α) < 28.17°; total reflections, 18,450; unique reflections, 4373 [R_{int} = 0.0767]; final R indices for all data, R_1 = 0.0585, $_wR_2$ = 0.1127. The structure solution and refinements were done using the SHELXTL package of crystallographic programs (version 5, 1994; G. M. Sheldrick, Siemens Analytical Xray Systems Inc., Madison, WI).
17. Electronic band structure calculations at the density functional theory level are under way (P. Larson, S. D. Mahanti, D.-Y. Chung, M. G. Kanatzidis, in preparation).
18. Fractional atomic coordinates (×10^4) and equivalent atomic displacement parameters (10^3 Å^2) for $CsBi_4Te_6$ with estimated standard deviations in parentheses (atom, x, y, z, B_{eq}) are as follows: Bi(1), 1362(1), 0, 7502(1), 17(1); Bi(2), 2124(1), 5000, −888(1), 18(1); Bi(3), 1628(1), 0, 921(1), 18(1); Bi(4), 886(1), 5000, −627(1), 18(1); Bi(5), 2353(1), 5000, −7410(1), 17(1); Bi(6), 1146(1), 5000, 2782(1), 17(1); Bi(7), 150(1), 0, 7878(1), 18(1); Bi(8), 396(1), 0, 1365(1), 18(1); Cs(1), 543(1), 0, 5090(1), 26(1); Cs(2), 3130(1), 0, −5163(1), 28(1); Te(1), 1533(1), 5000, −722(1), 14(1); Te(2), 800(1), 0, 7845(1), 16(1); Te(3), 1226(1), 5000, 6089(1), 18(1); Te(4), 2020(1), 0, 7561(1), 16(1); Te(5), 2250(1), 0, 766(1), 14(1); Te(6), 1043(1), 0, 1003(1), 15(1); Te(7), 1757(1), 5000, −7570(1), 16(1); Te(8), 1236(1), 0, 4213(1), 18(1); Te(9), 2396(1), 0, −5982(1), 18(1); Te(10), 575(1), 5000, 2811(1), 18(1); Te(11), −76(1), 5000, 3592(1), 19(1); Te(12), 322(1), 5000, −383(1), 17(1).
19. G. A. Slack, in *CRC Handbook of Thermoelectrics*, D. M. Rowe, Ed. (CRC Press, Boca Raton, FL, 1995), p. 407; G. A. Slack, in *Solid State Physics*, H. Ehrenreich, F. Seitz, D. Turnbull, Eds. (Academic Press, New York, 1997), vol. 34, p. 1.
20. J. W. Lyding, H. O. Marcy, T. J. Marks, C. R. Kannewurf, *IEEE Trans. Instrum. Meas.* **37**, 76 (1988).
21. Variable-temperature (4.2 to 295 K) thermopower data were taken using a slow-ac measurement technique. The measurement apparatus featured Au (0.07% Fe)/Chromel differential thermocouples for monitoring the applied temperature gradients. Samples were mounted on 60-μm gold wire using gold paste. Fine gold wire (diameter 10 μm) was used for sample voltage contacts, which were made as long as possible to minimize thermal conduction through the leads. The sample and thermocouple voltages were measured using Keithley Model 181 and Model 182 nanovoltmeters, respectively. The applied temperature gradient was about 0.1 to 0.4 K. Measurements were taken under a turbo-pumped vacuum maintained below 10^{-5} torr. The sample chamber was evacuated for at least 1 hour before cooling to remove any residual water vapor or solvents in the gold paste.
22. The density of oriented ingots is >99% of theoretical density. The thermal conductivity was measured along the growth direction, which is the direction of maximum TE performance.
23. H. J. Goldsmid and J. W. Sharp, *J. Electron. Mater.* **28**, 869 (1999)..
24. No significant variations (to ±10%) in thermal conductivity were observed between hot-pressed and oriented ingot samples.
25. *Encyclopedia of Materials Science and Engineering* (MIT Press, Cambridge, MA, 1986), p. 4968.
26. C. Kittel, in *Introduction to Solid State Physics* (Wiley, New York, ed. 6, 1986), p. 150.
27. M. V. Vedernikov, V. A. Kutasov, L. N. Luk'yanova, P. P. Konstantinov, in *Proceedings of the 16th International Conference on Thermoelectrics* (Dresden, Germany, 1997), p. 56.
28. H. Süβmann and W. Heiliger, in *Proceedings of the Conference on Transport in Compound Semiconductors* (MLU, Halle, Germany, KTB series 1982), p. 100.
29. P. Larson, S. D. Mahanti, D.-Y. Chung, M. G. Kanatzidis, in preparation.
30. Supported by Office of Naval Research grant N00014-98-1-0443. The work made use of the SEM facilities of the Center for Electron Optics at Michigan State University. The work at Northwestern made use of the Central Facilities supported by NSF through the Materials Research Center (grant DMR-9632472). We thank S. D. Mahanti for fruitful discussions.

20 September 1999; accepted 10 December 1999

Physics of Iron at Earth's Core Conditions

A. Laio,[1] S. Bernard,[2] G. L. Chiarotti,[1]* S. Scandolo,[1,3] E. Tosatti[1,3]

The bulk properties of iron at the pressure and temperature conditions of Earth's core were determined by a method that combines first-principles and classical molecular dynamic simulations. The theory indicates that (i) the iron melting temperature at inner-core boundary (ICB) pressure (330 gigapascals) is 5400 (±400) kelvin; (ii) liquid iron at ICB conditions is about 6% denser than Earth's outer core; and (iii) the shear modulus of solid iron close to its melting line is 140 gigapascals, consistent with the seismic value for the inner core. These results reconcile melting temperature estimates based on sound velocity shock wave data with those based on diamond anvil cell experiments.

Iron is thought to be the main constituent of Earth's solid inner core and liquid outer core. However, the bulk properties of Fe at such extreme physical conditions remain uncertain, including (i) the Fe melting temperature T_m at the pressure of the ICB (330 GPa) (*1–6*); (ii) the density of liquid Fe at T_m, which is needed to determine whether elements lighter than Fe are present in the outer core (*7–10*); and (iii) the elastic behavior of solid Fe close to the melting line (*11–14*).

The Fe melting temperature at high pressures has been determined by diamond anvil cell (DAC) and shock wave experiments (*1–6*). Recent DAC estimates of the melting line extend to 190 GPa (*3*) and agree with each other (*5, 6*) within 500 K. Shock wave–based estimates are available at ~240 GPa, but these result in a wider range of possible melting temperatures of 5800 K (*1*), 6700 K (*2*), and 6350 K (*4*). All of the shock wave–based estimates for T_m are inconsistent with the extrapolation of the Fe melting line from static DAC experiments (*3*), which predict a T_m of ~4000 K at 240 GPa.

We calculated the properties of Fe by a method that combines first-principles and classical molecular dynamics (MD) simulations. A correct account of the electronic structure of Fe at the ab initio level is fundamental for an accurate and reliable description of the properties of Fe at Earth's core conditions (*13, 15–17*). Our calculations were based on a finite-temperature extension of density-functional theory within the gradient-corrected local density approximation (GC LDA) (*18*) and on a pseudopotential description of the valence electron interaction with the ion core (nucleus plus 1s, 2s, and 2p atomic core states) (*19*). The calculated low-temperature pressure-density curve for hexagonal close-packed (hcp) Fe agrees with the x-ray data (*20*) (first-principles densities are ~1% smaller than experimentally determined densities at all pressures).

First-principles quality information on the high-temperature properties of Fe (melting properties, elasticity, diffusion, and Hugoniot equation of state) was obtained in this work by constructing classical potentials with an explicit dependence on the thermodynamic pressure-temperature (P-T) condition, exactly mimicking the first-principles MD at that P-T point. The potential, which includes non–two-body terms (*21, 22*) and angular forces (*22*), is optimized by matching the classical and first-principles forces and stresses with a self-consistent iterative procedure (*23*). Thermodynamic properties at that P-T condition are then extracted from classical MD simulations. The optimal potential (OP) constructed in this way will not be transferable to a different P-T condition, where a different potential must be constructed. Our approach is thus different from previous attempts to estimate the melting temperature

[1]International School for Advanced Studies and Istituto Nazionale per la Fisica della Materia, Via Beirut 2/4, I-34014 Trieste, Italy. [2]Commissariat à l'Energie Atomique, DRIF, BP 12, F-91680 Bruyères la Châtel, France. [3]International Centre for Theoretical Physics, I-34014 Trieste, Italy.

*To whom correspondence should be addressed. E-mail: guido@sissa.it